Nanoscale

PAPER

View Article Online
View Journal | View Issue

Cite this: *Nanoscale*, 2019, **11**, 15216

Whisky tasting using a bimetallic nanoplasmonic tongue†

Gerard Macias,‡[a] Justin R. Sperling, ‡[a] William J. Peveler, [b] Glenn A. Burley, [c] Steven L. Neale [a] and Alasdair W. Clark *[a]

Received 29th May 2019,
Accepted 26th June 2019

DOI: 10.1039/c9nr04583j

rsc.li/nanoscale

Metallic nanostructures are ideal candidates for optical tongue devices thanks to their chemical stability, the sensitivity of their plasmonic resonance to environmental changes, and their ease of chemical-functionalization. Here, we describe a reusable optical tongue comprising multiplexed gold and aluminum nano-arrays: a bimetallic device which produces two distinct resonance peaks for each sensing region. Through specific modification of these plasmonic arrays with orthogonal surface chemistries, we demonstrate that a dual-resonance device allows us to halve sensor sizes and data-acquisition times when compared to single-resonance, monometallic devices. We applied our bimetallic tongue to differentiate off-the-shelf whiskies with >99.7% accuracy by means of linear discriminant analysis (LDA). This advance in device miniaturization, functionalization, and multiplexed readout indicates nanoplasmonic tongues will have future applications in chemical mixture identification in applications where portability, reusability, and measurement speed are key.

1. Introduction

Today's electronic sensing devices are designed to resemble and enhance the biological senses.[2] Photodetectors,[3–5] pressure and temperature sensors,[6,7] and microphones[9] can be related to the biological counterparts of vision, touch, and hearing, respectively. However, there are still two senses that are extremely challenging to replicate: smell and taste, both of which are essential when it comes to detecting individual components in complex chemical mixtures or differentiating and grouping different mixtures.[10,11]

Chromatography is the current gold-standard for detection, identification, and classification of chemical components from complex gas[12] and liquid[13] mixtures. However, the nature of chromatographic identification techniques (such as liquid chromatography mass spectrometry) requires specialized laboratory equipment for the separation and analysis of a sample's chemical components. This results in costly, time-consuming, and often low throughput processes[14] that are unsuitable for applications where real-time monitoring or portability are desirable (air and liquid sampling in the security, food, or drug sectors, for example). In response to these issues artificial 'tongues' and 'noses' consisting of multiple, cross-reacting sensing elements have been developed.[10,15–19] Compared to the aforementioned laboratory-based tools,[12,13] these devices are portable, highly sensitive,[20] do not require component isolation, and can be fabricated relatively cheaply.[21,22]

Our perceptions of taste and smell rely on multiple partially-selective chemoreceptors that result in distinct electrochemical patterns for specific flavors and odors.[23] Influenced by this mechanism, artificial tongues/noses work by combining the responses of multiple cross-reactive sensors, allowing them to identify chemical mixtures through trained pattern recognition[15,20] rather than by measuring absolute concentrations of specific components within the mixture.[20,24,25] The more sensing regions added to the analysis, the more potential the device has to differentiate between mixtures.[26] Pattern-recognition sensors such as these are extremely versatile and have found applications in medical diagnostics,[16,27–31] environmental monitoring,[32,33] and food-safety.[10,17,34]

[a]*School of Engineering, University of Glasgow, Rankine Building, Oakfield Avenue, Glasgow, UK. E-mail: Alasdair.clark@glasgow.ac.uk*
[b]*School of Chemistry, University of Glasgow, Joseph Black Building, Glasgow, UK, G12 8QQ*
[c]*WestCHEM & Department of Pure & Applied Chemistry, University of Strathclyde, 295 Cathedral Street, Glasgow, G1 1XL, UK. E-mail: glenn.burley@strath.ac.uk*

†Electronic supplementary information (ESI) available: Simulations to determine nanostructure periodicity and the effect of the distance between metallic arrays in the bimetallic regions; SEM images of each of the fabricated devices; transmission response showing the effect of different surface chemistries on sensing devices in water; sample of the data matrix used for PCA and LDA analyses; PCA figures for organic solvent differentiation; PCA figures and PC coefficients for whisky differentiation; LDA figures for whisky differentiation. See DOI: 10.1039/c9nr04583j

‡These authors contributed equally to this work.

A wide variety of materials have been used in order to construct artificial pattern-recognition sensors, including fluorescent polymers, doped metal oxides, and olfactory proteins.[25,35,36] Recently, surface formed plasmonic gold (Au) nanostructures have emerged as a particularly useful sensing platform for these systems thanks to their chemical stability, the sensitivity of their plasmonic resonance to environmental changes, their ease of chemical-functionalization, and their reusability in comparison to solution phase sensing arrays.[37,38] The optical response of Au nanostructures is dictated by their localized surface plasmon resonance (LSPR), a phenomena particularly sensitive to changes in local refractive index.[39] Partial-selectivity in these devices is achieved by using multiple arrays of nanostructures, each modified with a different surface-chemistry, as individual sensing regions. When exposed to the same solution, the resonance peak-shift of each region varies due to the particular local chemical modification. Monitoring these variations results in the desired "fingerprint" for that mixture.[31] However, the need for multiple sensing regions inevitably impacts device size and measurement times. As a result, there are size, weight, and speed advantages associated with reducing the number of sensing regions required for mixture classification.

Here, we present a reusable optical tongue device with three sensing regions, where each region is capable of obtaining two partially selective responses from a single measurement. Each region consists of two superimposed nanoplasmonic arrays featuring two distinct metals: Au and aluminum (Al). This allows for the orthogonal chemical-functionalization of each superimposed array *via* thiol (Au)[40–42] and silane (Al)[41,43] chemistries, while also allowing us to obtain two resonance peak-shifts using a single optical measurement. Compared to a device containing its monometallic counterparts, we demonstrate that our device containing bimetallic Au/Al sensors can halve the number of sensing elements required (reducing device size and number of regions to probe [*i.e.* data acquisition time]) without compromising the identification and classification capabilities of the device. We go on to show that these sensors can be used as an optical tongue to distinguish between seven different whiskies and three controls.

2. Experimental

2.1 Device fabrication

Devices were fabricated using electron-beam lithography and metal-evaporation. Nanosquares of 100 nm × 100 nm, with a 300 nm period in X and Y, were patterned into a resist bi-layer of poly(methyl methacrylate) (PMMA) resist 2010 and PMMA 2041 (total thickness 150 nm) using a Vistec VB6 Ultra High Resolution Extra Wide Field electron beam lithography tool. Following development of the pattern, a 2/50 nm Ti/Au layer was evaporated onto the sample using a Plassys MEB 400S/550S electron-beam evaporation tool. These fabrication steps were then repeated to add 50 nm thick Al nanostructures.

2.2 Surface functionalization

The bimetallic device consisted of 3 Al/Au nanoarray regions. To create different localized environments for each region of the device, surface chemistry modifications were made. The first array consisted of unmodified Au and Al (with its native oxide layer). For these arrays, the base substrate was borosilicate glass (Fig. 2a(i)). For the second array, exposed sensor regions were immersed in a 10 mM ethanolic solution of 1-decanethiol (DT, Sigma-Aldrich) for 24 hours, rinsed three times with ethanol and dried with nitrogen. Hexamethyldisilazane (HMDS, Sigma-Aldrich) was then spun on at 4000 RPM for 60 seconds, allowed to air-dry for 2 minutes, and the excess was washed off. This produced the Au-DT and Al-HMDS surfaces (Fig. 2a(ii)). For these regions, the base substrate was modified to glass-HMDS. For the third set of chemistries, exposed sensor regions were immersed in a 10 mM ethanolic solution of 1*H*,1*H*,2*H*,2*H*-perfluoro-1-decanethiol (PFDT, Sigma Aldrich) for 24 hours, rinsed three times with ethanol and dried with nitrogen. The exposed regions were then immersed in a 0.5% solution (by volume) of 2-[methoxy(polyethyleneoxy)$_{6-9}$propyl] trimethoxysilane (PEG, Sigma-Aldrich) in toluene for 1 hour, rinsed three times with toluene, followed by rinsing three times with deionised water. The substrate was then nitrogen dried, and oven-baked at 100 °C for 30 minutes to produce the Au-PFDT and Al-PEG surfaces (Fig. 2a(iii)). For these regions, the base substrate was modified to glass-PEG. A monometallic device consisting of 6 nanoarray regions (3 Al and 3 Au) was fabricated for comparison. The same surface modifications were made to create the six sensing regions of Al, Au, Al-HMDS, Au-DT, Al-PEG, and Au-PFDT. Shifts of the transmission spectra (in water) from surface chemistry modifications are shown in Fig. S4, ESI.†

2.3 Solution preparation

Solutions of 10%, 20%, and 30% acetone (by volume) and 10%, 20%, 30%, and 40% ethanol (by volume) in deionised water were prepared. The selection of whiskies and vodka in Table 1 were purchased from their respective distilleries.

2.4 Experimental setup

The sensor arrays were enclosed in a polydimethylsiloxane (PDMS) chamber. These chambers were then filled with each test solution agitated for 2 minutes. A custom-built microspectrophotometer was used to measure the real-time transmission spectra (0.5 nm resolution). Light from a VIS-NIR light source (tungsten-halogen 400 to 1200 nm wavelength) was used to probe each element of the sensor. A 10× objective was used to couple the transmitted light into an optical-fiber attached to a StellarNet Microspectrophotometer (StellarNet Blue Wave). With this objective, the spot size of the optical fiber is around 45 μm. For ease of measurement, each element in the sensor was thus fabricated to be 300 μm^2 in size. For the acetone and ethanol solvent differentiation, three different preparations of each solvent were made, and subsequent transmission spectra were taken. For the alcohol differentiation experimentation, thirty transmission spectra per sensor

Table 1 Alcohols tested in the whisky tongue

ID	Name	Serial number	%	Type	Region	Barrel	Malt	Age
0○	DI H_2O	—	0	Deionized water	—	—	—	—
E○	40% Ethanol in DI H_2O (v/v)	—	40	Deionized water/ ethanol mixture	—	—	—	—
V◊	Absolut®	L20180109H16:07	40	Vodka	—	—	—	—
W1+	Glenfiddich® 12 years	L33B465421080841	40	Scotch Whisky	Speyside	Amer. Oak /Eur. Sherry	Single	12
W2△	Glenfiddich® 15 years	L33B446630051142	40	Scotch Whisky	Speyside	Eur. Sherry /Solera Vat	Single	15
W3◊	Glenfiddich® 18 years	L33B462719071531	40	Scotch Whisky	Speyside	Amer. Oak /Span. Oloroso	Single	18
W4+	Glen Marnoch® Sherry Cask	LBB6B1406021117 15:44	40	Scotch Whisky	Highland	Amer. Oak /Eur. Sherry	Single	—
W5△	Glen Marnoch® Bourbon Cask	LBB6B1405021117 19:42	40	Scotch Whisky	Highland	Amer. Oak /Bourbon	Single	—
W6◊	Glen Marnoch® Rum Cask	LBB6B1407021117 17:53	40	Scotch Whisky	Highland	Amer. Oak /Caribbean Rum	Single	—
W7◊	Laphroaig® 10 years	L6262MB222990853	40	Scotch Whisky	Islay	Bourbon	Single	10

region, for each solution, were measured. Between measurements, samples were rinsed in water, then ethanol, and nitrogen dried. A baseline measurement of a "blank" region the sample was used prior to measuring an element in one of the tongue arrays for background correction.

2.5 Data analysis

MATLAB was used to analyze the transmission spectra. The transmission spectrum was smoothed (20 points, mean-average smoothing) and interpolated (from 0.5 nm to 0.01 nm). The peak position value of the minima peaks (one for each monometallic element and two for each bimetallic element) was determined. The resulting transmission peak values (wavelength in nanometers) were arranged in a data matrix, where the rows of the matrix corresponded to a particular solution and the columns corresponded to the wavelength of the resonant peaks for each chemistry- Au, Al, Au-DT, Al-HMDS, Au-PFDT, Al-PEG. The data matrix was first analyzed using the inherent principal component analysis (PCA) function in MATLAB (by singular value decomposition algorithm). The variance for the scree plot was obtained from the MATLAB PCA result set. Linear discriminant analysis (LDA) was then performed on the same data matrix using Systat 13 software. An example of the data matrix and further information on the PCA and LDA techniques can be found in the ESI.†

3. Results and discussion

Our bimetallic sensor consists of two arrays of square nanostructures organized in a "checkerboard"-like arrangement; one array constructed with Au, the other with Al. This configuration was chosen so that the device displayed two well-resolved peaks in the visible spectrum, with low transmission at their respective minima (design optimization details can be found in the ESI†). The bimetallic sensor was fabricated on a borosilicate-glass substrate *via* a multi-step electron-beam lithography process. Fig. 1a shows SEMs of (i) monometallic Al, (ii) monometallic Au, and (iii) bimetallic Al/Au. In the SEM images, the two metals can be differentiated due to their distinct electron scattering properties, Au being 'brighter' than Al.[44] Fig. 1b shows a typical transmission spectrum for a bimetallic sensor (solid, black line) compared to equivalent

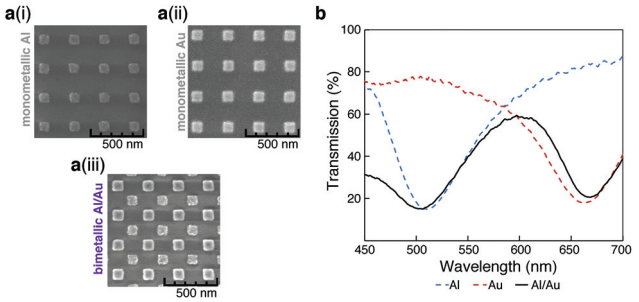

Fig. 1 Comparison of mono- and bimetallic LSPR sensors. (a) SEMs showing (i) monometallic Al, (ii) monometallic Au, and (iii) bimetallic Al/Au regions. (b) Transmission response of arrays of Al-only (dotted-blue), Au-only (dotted-red), and bimetallic Al/Au (black solid) in water.

monometallic sensors of Al (dotted, blue line) and Au (dotted, red line). As confirmed by the spectra of the two monometallic sensors, the two peaks in the bimetallic transmission spectrum at 500 nm and 660 nm correspond to Al and Au, respectively.

Both Au and Al can support selective functionalization of their surfaces. While the Au nanostructures can be readily modified by thiol chemistry,[40–42] the native oxide layer present on the Al nanostructures displays –OH groups which enables modification *via* silane chemistry.[41,43] The presence of organic ligands on plasmonic arrays is known to influence the extent to which certain organic molecules interact with the arrays, thus affecting the refractive index around the nanostructures and in-turn their resonant properties.[37] While monometallic sensor arrays with single-ligand modifications have been reported,[31] bimetallic arrays that allow dual-ligand modifications have yet to be explored.

Our system comprised of 3 bimetallic sensor arrays, each exhibiting unique surface chemistries: a sensor consisting of native Au and Al (Fig. 2a(i)); a sensor where the Au was modified with DT (1-decanethiol) and the Al with HMDS (hexamethyldisilazane) (Fig. 2a(ii)); and a sensor where the Au was modified with PFDT (1*H*,1*H*,2*H*,2*H*-perfluoro-1-decanethiol) and the Al with PEG (2-[methoxy(polyethyleneoxy)$_{6-9}$propyl] trimethoxysilane) (Fig. 2a(iii)). These surface chemistries were chosen to represent varied levels of hydrophobicity/philicity and different chemical functionalities. Altering the surface chemistry of the

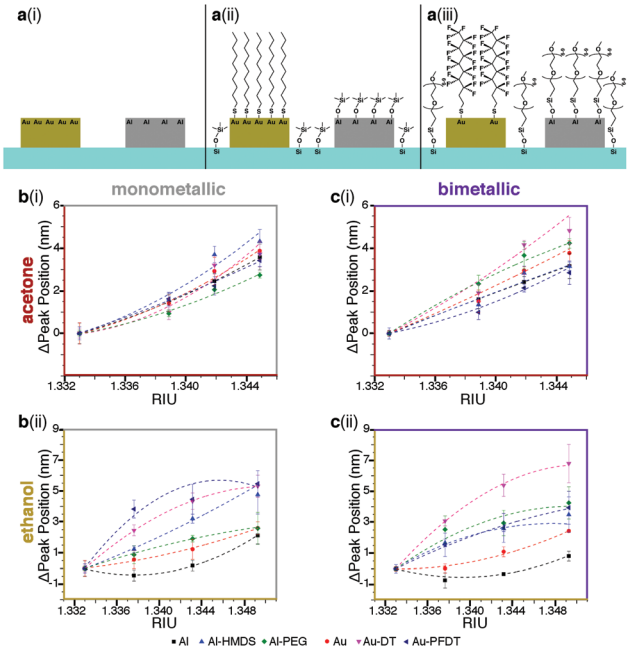

Fig. 2 Effect of surface chemistry on the sensitivity of Au, Al, and Au/Al sensor arrays. (a) Surface chemistry combinations used: (i) native Al, Au (ii) Al-HMDS, Au-DT, and (iii) Al-PEG, Au-PFDT. (b) The shift in plasmonic response from water for monometallic arrays in 10%, 20%, and 30% solutions (v/v) of (i) acetone and (ii) ethanol. (c) The shift in plasmonic response from water for bimetallic arrays in 10%, 20%, and 30% solutions (v/v) of (i) acetone and (ii) ethanol. The different surface chemistries (native Al, Al-HMDS, Al-PEG, native Au, Au-DT, and Au-PFDT) alter the plasmonic peak of the nanostructures when exposed to the same organic solvent. This results in different peak-shifted curves. The RIU values for acetone and ethanol solutions were obtained from S. S. Kurtz, *et al.* (1965)[1] and T. A. Scott (1946),[8] respectively. For (b) and (c), the lines are present to guide the eye and the error bars are one standard deviation from the average.

nanostructures affects how individual chemical components in a mixture interact with the structures, altering their optical response. In addition to this "bimetallic" sensor array, a corresponding array of 6 equivalent monometallic sensors of Au and Al were also produced, matching the chemistries used on the bimetallic sensors (*i.e.* 3 Au arrays and 3 Al arrays). The monometallic (Fig. 2b) and bimetallic (Fig. 2c) sensors were tested against varying refractive index media adjusted with (i) acetone and (ii) ethanol. The resulting resonance shifts from water (RIU = 1.333) were compared using RIU values for acetone[1] and ethanol[8] solutions.

Three trends were identified:

(1) Regardless of the metallic composition of the nanostructures, the organic solvent used to modify the refractive index, or whether the region is monometallic or bimetallic, the sensitivity curve depends on the organic ligand present on the nanostructure (*e.g.*, the Al, Al-HMDS, and Al-PEG curves in Fig. 2b(i) are different).

(2) For any given surface chemistry on either the monometallic or bimetallic sensor, the sensitivity curve depends on the type of organic solvent used to alter the refractive index rather than just shifting with RIU alone (*e.g.* the Al-HMDS curves in Fig. 2b(i) and (ii) are not the same.)

(3) The sensitivity curves of the monometallic and bimetallic sensor for the same metal composition, organic ligand, and organic solvent, differ; the bimetallic sensors response is fundamentally different from its monometallic counterparts (*e.g.* the Al-HMDS sensitivity curves in Fig. 2b(i) and c(i) are not the same.)

In all three cases, we attribute these behaviors to the segregation of the solvent at the sensor-liquid interface and corresponding changes to the local refractive index. Solvent segregation is dependent on the chemical groups present at the interface;[45] using different metals and different ligands on the surface results in different segregation behavior, which likely explains the different plasmonic responses. This is especially important when comparing the monometallic and bimetallic responses; the presence of a second metal and second ligand results in additional differential solvent segregation behavior. These results confirm that we can tailor the partial selectivity of the device *via* the orthogonal silane and thiol chemistry.

To further verify the applicability of the bimetallic approach for implementation as an optical tongue device, we performed a principal component analysis (PCA – a non-biased, multivariant analysis technique)[19,46] across 10 different bimetallic 'tongues' using the data from our acetone/ethanol test. Each bimetallic tongue consisted of three element pairs: Al/Au, Al-HMDS/Au-DT, and Al-PEG/Au-PFDT. For the PCA, each row corresponded to a particular solvent tested, and each column corresponded to the transmission peak minimum for each surface chemistry. Further explanation of the PCA analysis used can be found in the Data Matrix for Analysis section of the ESI.†

Fig. 3 shows the PCA of the first two principal components (that explain 87.3% of the total variance), where black dots rep-

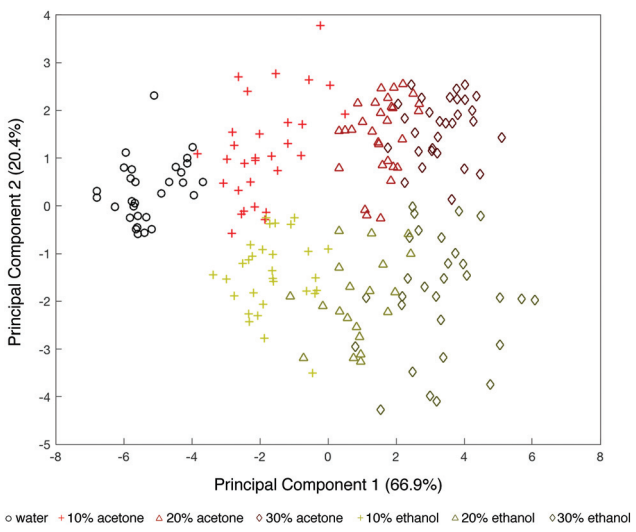

Fig. 3 PCA for organic solvent differentiation. The transmission peaks of 10 bimetallic devices (30 sensing regions) in 10%, 20%, and 30% acetone and ethanol solutions were used to generate a PCA with each sensor as a new row of the PCA.

resent DI water, red dots represent acetone-based media and yellow dots represent ethanol-based media. These results show that by combining the response of multiple surface chemistries on our bimetallic sensors, we are able to cluster the results from each solution into a map.

While delineation of classes (acetone/ethanol and the v/v percent of each) is shown, it is important to note that this PCA analyzed the results across 10 different optical tongue devices. A close look at SEM images of each of these devices revealed that, while within the specifications of our e-beam lithography tool (*i.e.* 20 nm spatial resolution), the *X*–*Y* distances between our two metals was slightly different in each device (see ESI†). Given the high sensitivity of plasmonic nanostructures to their near-field environment, such minute misalignments can result in slight differences from sensor to sensor[47,48] (confirmed by simulations Fig. S3, ESI†). Additionally, variations in position between the Al and Au arrays can alter the surface wettability and segregation properties. This is because the distribution of hydrophobic and hydrophilic groups is dependent on the position of the metals and their uniquely modified surface chemistries within the array.[49] Thus, the spread of points within each class in the PCA is most likely attributed to this fabrication resolution. Regardless, the PCA shows ordering of the different solutions by combining the response from three sensing regions, which constitutes the basic requirement for the development of an artificial tongue. Similar behavior was observed with comparable monometallic sensors (six sensing regions) and can be found in the ESI.†

To further demonstrate the capabilities of the bimetallic tongue, we used one device to differentiate between seven different whiskies with identical ethanol contents (40%), a 40% vodka, and 40% ethanol in water, with water as the control (as shown in Table 1). This test was performed on a single bimetallic array to minimize the variance between sensors that would increase the noise within the data. The resulting response of the bimetallic array was compared to an equivalent monometallic array (containing six sensing regions). Fig. 4a(ii) and b(ii) show the 2D PCA results for the monometallic and bimetallic tongues, respectively. These PCAs show only the alcoholic solutions; water is off the axis set. Full PCAs can be viewed in the ESI.†

Sensor performance is determined by the dimensionality of the PCA, the distance between the groupings, and 'tightness' of the groupings. The dimensionality is measured by the number of components required to account for 95% of measurement variance, as shown in Fig. 4a(iii) and b(iii). For the plasmonic tongue comprised of six monometallic sensors, two dimensions (principal components) contained >95% variance; and for the plasmonic tongue comprised of three bimetallic sensors, the first two principal components (PCs) contained 94.6% variance (with >95% of the variance over three dimensions). The overall difference between the cumulative variance of monometallic and bimetallic tongues with two principal components is very small. In both cases, the important qualitative point is that the PCA algorithm shows distinct

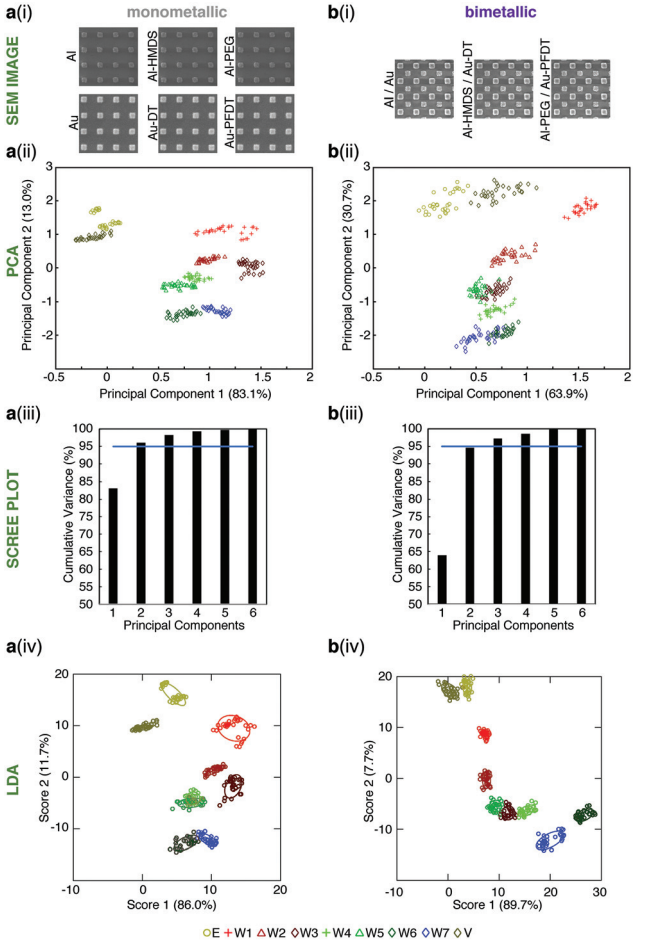

Fig. 4 Monometallic *versus* bimetallic tongues for whisky differentiation. Results for (a) monometallic and (b) bimetallic sensor arrays for the differentiation of the solutions found in Table 1. For each full tongue device: (i) SEM showing the make-up of each tongue device, (ii) PCA zoomed in to show only the alcoholic solutions; (iii) the PCA scree plot; and (iv) LDA zoomed in to show only the alcoholic solutions. The confidence ellipses for the LDA are one standard deviation. The colors used in the PCA and LDA are identified by the first column of Table 1. Full PCA and LDA figures can be found in the ESI.†

differentiation of the different test solutions with large spacings between these groupings.

In both PCA analyses (mono- *versus* bimetallic) the pattern of water *versus* whisky and ethanol/vodka *versus* whisky is largely similar. W1 (Glenfiddich® 12y) in particular gives a markedly different signal to the other spirits tested. Analysis of the PCs in each tongue give an indication of the elements contributing to the sensor response. As shown in Table S3 (ESI†), for the monometallic tongue, PC1 is from the transmission peaks corresponding to the Au nanostructures, particularly Au and Au-PFDT that separate water from ethanolic solutions. Al-HDMS contributes to the PC2, along with Al which has the most separation of the whiskies/controls. In the bimetallic tongue, many chemical functionalities contribute to the PC1, leading to the separation of the water and whiskies as well as improved separation between vodka and ethanol solution, but

PC2 is dominated by Al and Al-PEG, demonstrating that by combining the surface chemistries in a single device, different behavior is observed.

In this sensor configuration we hypothesize that whilst the main driver in the solution fingerprints is clearly the EtOH content (*vs.* water), the trace differences between a pure EtOH solution and the compounds present in the spirits are causing significant signal variations. These compounds include the additional alcohols present in whiskies (propanols and butanols), organic aromatic components (phenols, terpenes and vanillin), and aliphatics (lactones). Each of these components will have different interactions with the sensor surface coatings dependent on their partial solubility and hydrophobicitiy/phillicity. It is proposed the most hydrophilic components will interact favorable with the bare Al and PEG surfaces, whilst the most hydrophobic will prefer to interact with the Au and Au-DT surfaces. Factors such as pH or ionic strength may also contribute to the subtle changes seen on the sensor chips.

After analyzing the PCA and discrimination capabilities of both mono- and bimetallic tongues, we can conclude that both tongues are able to differentiate between the whiskies tested thanks to the functional groups present on their surface. To investigate whether formal classification was possible, linear discriminant analysis (LDA), a supervised technique, was applied to the data to generate new "scores" (in a similar methodology to PCA) to maximize separation between known clusters whilst minimizing variance within each cluster.[50] Both the mono- (Fig. 4a(iv)) and bimetallic (Fig. 4b(iv)) tongues performed excellently and could classify (using leave-one-out cross validation to test accuracy) 100% and 99.7% of the data, respectively. Although the bimetallic tongue confused one instance of W3 for W5, this was arguably compensated for by its ability to provide two signals from one measurement and therefore make half the number of measurements required to collect the data, requiring less sample volume. Additionally, the greater cross-reactivity on these sensor elements increases the potential for tuning and improving the fingerprint responses by incorporating different pairings of surface chemistry.

4. Conclusions

We have presented a reusable bimetallic nanoplasmonic tongue that displays two distinct resonance peaks per region and whose orthogonal surface chemistries can be selectively modified to tune their 'tasting' sensitivity. These unique features have allowed us to halve both the sensor size and necessary data-acquisition time while still providing dataset clustering upon PCA and successful classification with LDA. This is a versatile system, allowing the development of high quality nanoplasmonic tongues for any given application *via* simple alterations to the chosen surface ligands and/or plasmonic metals in order to produce new sensors with unique chemical responses. This new approach to artificial tongue design may spur the development of portable devices for applications in a point of care diagnostics, counterfeit detection in high-value drinks, environmental monitoring, and defense.

Conflicts of interest

There are no conflicts to declare.

Author contributions

All authors conceived and designed the experiments. All authors contributed to the writing and editing of the manuscript. G.M. and J.R.S. simulated, designed, and fabricated the devices, and performed the experiments. G.M., J.R.S. and W.J. P. evaluated the data. J.R.S. and G.M. contributed equally to the work. A.W.C., S.L.N., and G.A.B. coordinated and supervised the work. All authors have given approval to the final version of the manuscript.

Acknowledgements

This work was supported by The Leverhulme Trust (grants RPG-2014-343 and RPG-2018-149), EPSRC (grant EP/P51133X/1), and BBSRC (grant BB/N016734/1). W. J. P. thanks the University of Glasgow for a Lord Kelvin Adam Smith Fellowship. The authors also wish to thank all the staff working in the James Watt Nanofabrication Centre for their support.

Notes and references

1 S. S. Kurtz, A. Wikingss, D. L. Camin and A. R. Thompson, Refractive index and density of acetone-water solutions, *J. Chem. Eng. Data*, 1965, **10**(4), 330–334.
2 M. del Valle, Bioinspired Sensor Systems, *Sensors*, 2011, **11**(11), 10180–10186.
3 F. Stockmann, Photodetectors, their performance and their limitations, *Appl. Phys.*, 1975, **7**(1), 1–5.
4 E. Laux, C. Genet, T. Skauli and T. W. Ebbesen, Plasmonic photon sorters for spectral and polarimetric imaging, *Nat. Photonics*, 2008, **2**(3), 161–164.
5 X. Dong, X. Huang, Y. Zheng, L. Shen and S. Bai, Infrared dim and small target detecting and tracking method inspired by Human Visual System, *Infrared Phys. Technol.*, 2014, **62**, 100–109.
6 D. J. Lipomi, M. Vosgueritchian, B. C. K. Tee, S. L. Hellstrom, J. A. Lee, C. H. Fox, *et al.*, Skin-like pressure and strain sensors based on transparent elastic films of carbon nanotubes, *Nat. Nanotechnol.*, 2011, **6**(12), 788–792.
7 V. J. Lumelsky, M. S. Shur and S. Wagner, Sensitive Skin, *IEEE Sens. J.*, 2001, **1**(1), 41–51.
8 T. A. Scott, Refractive index of ethanol-water mixtures and density and refractive index of ethanol-water-ethyl ether mixtures, *J. Phys. Chem.*, 1946, **50**(5), 406–412.

9 Y. Zhang, R. Bauer, J. C. Jackson, W. M. Whitmer, A. F. C. Windmill and D. Uttamchandani, A Low-Frequency Dual-Band Operational Microphone Mimicking the Hearing Property of Ormia Ochracea, *J. Microelectromech. Syst.*, 2018, **27**(4), 667–676.

10 M. L. Rodriguez-Mendez, J. A. De Saja, R. Gonzalez-Anton, C. Garcia-Hernandez, C. Medina-Plaza, C. Garcia-Cabezon, *et al.*, Electronic Noses and Tongues in Wine Industry, *Front. Bioeng. Biotechnol.*, 2016, **4**(81), 1–12.

11 L. Guerrini, E. Garcia-Rico, N. Pazos-Perez and R. A. Alvarez-Puebla, Smelling, Seeing, Tasting-Old Senses for New Sensing, *ACS Nano*, 2017, **11**(6), 5217–5222.

12 W. Jennings and T. Shibamoto, *Qualitative Analysis of Flavor and Fragrance Volatiles by Glass Capillary Gas Chromatography*, Elsevier, 1 edn, 2012.

13 S. C. Ng, T. T. Ong, P. Fu and C. B. Ching, Enantiomer separation of flavour and fragrance compounds by liquid chromatography using novel urea-covalent bonded methylated beta-cyclodextrins on silica, *J. Chromatogr., A*, 2002, **968**(1–2), 31–40.

14 C. J. Welch, N. Wu, M. Biba, R. Hartman, T. Brkovic, X. Gong, *et al.* Greening analytical chromatography, *TrAC, Trends Anal. Chem.*, 2010, **29**(7), 667–680.

15 B. G. Kermani, S. S. Schiffman and H. T. Nagle, Performance of the Levenberg-Marquardt neural network training method in electronic nose applications, *Sens. Actuators, B*, 2005, **110**(1), 13–22.

16 A. D'Amico, G. Pennazza, M. Santonico, E. Martinelli, C. Roscioni, G. Galluccio, *et al.*, An investigation on electronic nose diagnosis of lung cancer, *Lung Cancer*, 2010, **68**(2), 170–176.

17 J. Han, C. Ma, B. Wang, M. Bender, M. Bojanowski, M. Hergert, *et al.*, A Hypothesis-Free Sensor Array Discriminates Whiskies for Brand, Age, and Taste, *Chem*, 2017, **2**(6), 817–824.

18 A. Mimendia, J. M. Gutierrez, L. Leija, P. R. Hernandez, L. Favari, R. Munoz, *et al.*, A review of the use of the potentiometric electronic tongue in the monitoring of environmental systems, *Environ. Model. Softw.*, 2010, **25**(9), 1023–1030.

19 J. R. Askim, M. Mahmoudi and K. S. Suslick, Optical sensor arrays for chemical sensing: the optoelectronic nose, *Chem. Soc. Rev.*, 2013, **42**(22), 8649–8682.

20 W. J. Peveler, M. Yazdani and V. M. Rotello, Selectivity and Specificity: Pros and Cons in Sensing, *ACS Sens.*, 2016, **1**(11), 1282–1285.

21 K. Persaud and G. Dodd, ANalysis of discrimination mechanisms in the mammalian olfactory system using a model nose, *Nature*, 1982, **299**(5881), 352–355.

22 C. Lu and R. H. Lipson, Interference Lithography: A Powerful Tool for Fabricating Periodic Structures, *Laser Photonics Rev.*, 2010, **4**(4), 568–580.

23 L. B. Vosshall and R. E. Stocker, Molecular architecture of smell and taste in Drosophila, *Annu. Rev. Neurosci.*, 2007, **30**, 505–533.

24 E. V. Anslyn and V. M. Rotello, Chemosensory models: approaches and applications of differential sensing Editorial overview, *Curr. Opin. Chem. Biol.*, 2010, **14**(6), 683–684.

25 Z. Li, J. R. Askim and K. S. Suslick, The Optoelectronic Nose: Colorimetric and Fluorometric Sensor Arrays, *Chem. Rev.*, 2019, **119**(1), 231–292.

26 K. L. Goodner, J. G. Dreher and R. L. Rouseff, The dangers of creating false classifications due to noise in electronic nose and similar multivariate analyses, *Sens. Actuators, B*, 2001, **80**(3), 261–266.

27 A. P. F. Turner and N. Magan, Electronic noses and disease diagnostics, *Nat. Rev. Microbiol.*, 2004, **2**(2), 161–166.

28 Y. Geng, W. J. Peveler and V. M. Rotello, Array-based "Chemical Nose" Sensing in Diagnostics and Drug Discovery, *Angew. Chem., Int. Ed.*, 2019, **58**(16), 5190–5200.

29 W. J. Peveler, R. F. Landis, M. Yazdani, J. W. Day, R. Modi, C. J. Carmalt, *et al.*, A Rapid and Robust Diagnostic for Liver Fibrosis Using a Multichannel Polymer Sensor Array, *Adv. Mater.*, 2018, **30**(28), 1800634.

30 W. Li, H. Liu, D. Xie, Z. He and X. Pi, Lung Cancer Screening Based on Type-different Sensor Arrays, *Sci. Rep.*, 2017, **7**, 1969.

31 G. Peng, M. Hakim, Y. Y. Broza, S. Billan, R. Abdah-Bortnyak, A. Kuten, *et al.*, Detection of lung, breast, colorectal, and prostate cancers from exhaled breath using a single array of nanosensors, *Br. J. Cancer*, 2010, **103**(4), 542–551.

32 W. J. Peveler, A. Roldan, N. Hollingsworth, M. J. Porter and I. P. Parkin, Multichannel Detection and Differentiation of Explosives with a Quantum Dot Array, *ACS Nano*, 2016, **10**(1), 1139–1146.

33 K. L. Diehl and E. V. Anslyn, Array sensing using optical methods for detection of chemical and biological hazards, *Chem. Soc. Rev.*, 2013, **42**(22), 8596–8611.

34 N. El Barbri, E. Llobet, N. El Bari, X. Correig and B. Bouchikhi, Electronic nose based on metal oxide semiconductor sensors as an alternative technique for the spoilage classification of red meat, *Sensors*, 2008, **8**(1), 142–156.

35 C. Wu, Y.-W. Du, L. Huang, Y. B.-S. Galeczki, A. Dagan-Wiener, M. Naim, *et al.*, Biomimetic Sensors for the Senses: Towards Better Understanding of Taste and Odor Sensation, *Sensors*, 2017, **17**(12), 2881.

36 W. J. Peveler, R. Binions, S. M. V. Hailes and I. P. Parkin, Detection of explosive markers using zeolite modified gas sensors, *J. Mater. Chem. A*, 2013, **1**(7), 2613–2620.

37 G. Peng, U. Tisch, O. Adams, M. Hakim, N. Shehada, Y. Y. Broza, *et al.*, Diagnosing lung cancer in exhaled breath using gold nanoparticles, *Nat. Nanotechnol.*, 2009, **4**(10), 669–673.

38 K. Saha, S. S. Agasti, C. Kim, X. Li and V. M. Rotello, Gold Nanoparticles in Chemical and Biological Sensing, *Chem. Rev.*, 2012, **112**(5), 2739–2779.

39 S. A. Maier, *Plasmonics: Fundamentals and Applications*, Springer Science+Business Media LLC, New York, 2007.

40 L. Srisombat, A. C. Jamison and T. R. Lee, Stability: A key issue for self-assembled monolayers on gold as thin-film coatings and nanoparticle protectants, *Colloids Surf., A*, 2011, **390**(1–3), 1–19.

41 C. Nicosia and J. Huskens, Reactive self-assembled monolayers: from surface functionalization to gradient formation, *Mater. Horiz.*, 2014, **1**(1), 32–45.

42 J. R. Sperling, G. Macias, S. L. Neale and A. W. Clark, Multilayered Nanoplasmonic Arrays for Self-Referenced Biosensing, *ACS Appl. Mater. Interfaces*, 2018, **10**(40), 34774–34780.

43 A. M. M. Jani, E. J. Anglin, S. J. P. McInnes, D. Losic, J. G. Shapter and N. H. Voelcker, Nanoporous anodic aluminium oxide membranes with layered surface chemistry, *Chem. Commun.*, 2009, (21), 3062–3064.

44 J. I. Goldstein, D. E. Newbury, J. R. Micheal, N. W. M. Ritchie, J. H. J. Scott and D. C. Joy, in *Scanning Electron Microscopy and X-Ray Microanalysis*, Springer, 4th edn, 2017.

45 J. T. Koberstein, Molecular design of functional polymer surfaces, *J. Polym. Sci., Part B: Polym. Phys.*, 2004, **42**(16), 2942–2956.

46 S. Wold, K. Esbensen and P. Geladi, Principal component analysis, *Chemom. Intell. Lab. Syst.*, 1987, **2**(1–3), 37–52.

47 L. Guo, J. A. Jackman, H.-H. Yang, P. Chen, N.-J. Cho and D.-H. Kim, Strategies for enhancing the sensitivity of plasmonic nanosensors, *Nano Today*, 2015, **10**(2), 213–239.

48 K. H. Su, Q. H. Wei, X. Zhang, J. J. Mock, D. R. Smith and S. Schultz, Interparticle coupling effects on plasmon resonances of nanogold particles, *Nano Lett.*, 2003, **3**(8), 1087–1090.

49 X. M. Liu, J. L. Thomason and F. R. Jones, *The Concentration of Hydroxyl Groups on Glass Surfaces and Their Effect on the Structure of Silane Deposits*, Silanes and Other Coupling Agents, 2009, vol. 5, pp. 25–38.

50 S. Stewart, M. A. Ivy and E. V. Anslyn, The use of principal component analysis and discriminant analysis in differential sensing routines, *Chem. Soc. Rev.*, 2014, **43**(1), 70–84.